New Limit on the Electron Electric Dipole Moment

B. C. Regan,* Eugene D. Commins,† Christian J. Schmidt,‡ and David DeMille§

Physics Department, University of California, Berkeley, California 94720
and Lawrence Berkeley National Laboratory, Berkeley, California 94720

(Received 8 August 2001; published 1 February 2002)

We present the result of our most recent search for T violation in ^{205}Tl, which is interpreted in terms of an electric dipole moment of the electron d_e. We find $d_e = (6.9 \pm 7.4) \times 10^{-28} e$ cm, which yields an upper limit $|d_e| \leq 1.6 \times 10^{-27} e$ cm with 90% confidence. The present apparatus is a major upgrade of the atomic beam magnetic-resonance device used to set the previous limit on d_e.

DOI: 10.1103/PhysRevLett.88.071805 PACS numbers: 13.40.Em, 11.30.Er, 14.60.Cd, 32.10.Dk

An intrinsic electric dipole moment (EDM) can exist only if parity (P) and time reversal (T) invariance are violated [1]. The weak interaction violates P, while CP violation (equivalent to T violation from CPT invariance) is observed in neutral kaon and B-meson decay [2]. Hence, the weak interaction and CP violation could induce EDMs by means of radiative corrections to the electromagnetic interaction. In the standard model intrinsic EDMs are much too small to be detected [3], but various extensions to the standard model predict observable values [4,5]. Sensitive searches [6,7] for EDMs constrain these models. In heavy paramagnetic atoms an electron EDM results in an atomic EDM enhanced by a factor $R \equiv d_{\text{atom}}/d_e$ [8]. We study atomic thallium in its $6^2P_{1/2}F = 1$ ground state, where $R \simeq -585$ [9].

Like its predecessor [10,11], the new experiment [12] uses magnetic resonance with two oscillating rf fields [13] separated by a space containing an intense electric field $\mathbf{E}$, and employs laser optical pumping for state selection and analysis. To control systematic effects from motional magnetic fields $\mathbf{E} \times \mathbf{v}/c$, the previous experiment employed a single pair of counterpropagating vertical atomic beams. The present experiment has two pairs separated by 2.54 cm, each consisting of Tl and Na (see Fig. 1). The spatially separated beams are nominally exposed to identical magnetic but opposite electric fields; this provides common-mode noise rejection and control of some systematic effects. Sodium serves as a comagnetometer: it is susceptible to the same systematic effects but insensitive to d_e, since R is roughly proportional to the cube of the nuclear charge. Also, Na's two $3^2S_{1/2}$ ground-state hyperfine levels $F = 2, 1$ have $g_F = \pm 1/2$, which permits the separation of two different types of $\mathbf{E} \times \mathbf{v}$ effects.

Figure 1 shows the apparatus with the up beams active. Atoms leave the trichamber oven thermally distributed among the ground state hyperfine levels. After some collimation they enter the quantizing magnetic field $\mathbf{B}$, nominally in the $\hat{\mathbf{z}}$ direction and typically 0.38 G. Laser beams then depopulate the states with nonzero magnetic quantum numbers m_F. Thus, in the first optical region 378 nm $\hat{\mathbf{z}}$ polarized light selects the $m_F = 0$ Zeeman sublevel of the Tl $F = 1$ ground state. In the second optical region 590 nm $\hat{\mathbf{z}}$ light selects the $m_F = 0$ sublevel of either the $F = 2$ or the $F = 1$ Na ground state. The first rf region contains an oscillating magnetic field $\mathbf{B}_{\text{rf}} = (B_{\text{Tl}} \cos\omega_{\text{Tl}} t + B_{\text{Na}} \cos\omega_{\text{Na}} t)\hat{\mathbf{x}}$, where $2B_{\text{Tl}} = B_{\text{Na}}$ and $1.506\omega_{\text{Tl}} \simeq \omega_{\text{Na}}$. These resonant fields apply "$\pi/2$" pulses, creating coherent superpositions of the $m_F \neq 0$ states of each species.

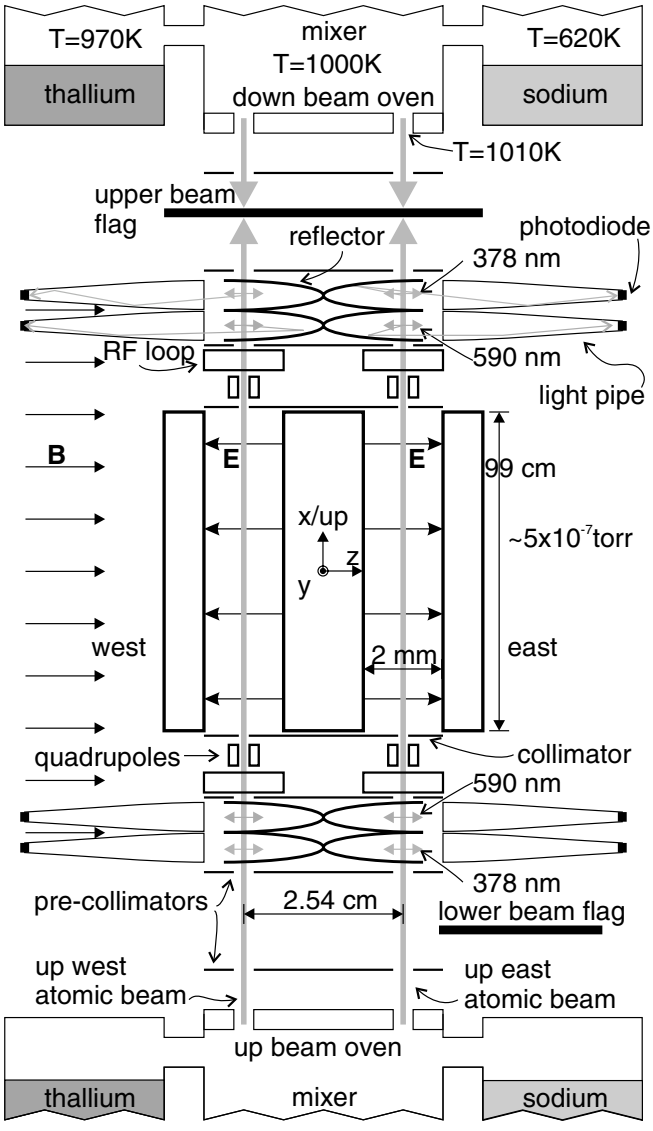

FIG. 1. Schematic diagram of the experiment; not to scale.

The atoms then move into the electric field, nominally parallel or antiparallel to $\mathbf{B}$. Typically $|\mathbf{E}| = 1.23 \times 10^5$ V/cm. The second rf field is coherent with the first, differing only by a relative phase shift α. In the analysis regions the atoms are probed with the same laser that performs the state selection. Fluorescence photons accompanying the atomic decays are reflected by polished aluminum paraboloids into Winston cones [14] made of UV-transmitting plastic. These light pipes are terminated by 1 cm^2 photodiodes.

The resulting signals are approximated by

$$S \simeq \sum_{k=0}^{2F} \left\langle A_k \cos\left[k\left(\omega T - \int_0^T \gamma |B|\, dt - \varepsilon + \alpha \right) \right] \right\rangle. \tag{1}$$

Here $\langle \cdots \rangle$ means integration over the beam velocity distribution and trajectories. Also $\gamma = |g_F \mu_B|/\hbar$, T is the time of transit between the two rf regions, and

$$\varepsilon \simeq \int_0^T \left[\frac{R d_e}{\hbar} \frac{\mathbf{B}\cdot\mathbf{E}}{|\mathbf{B}|} + \frac{\gamma \mathbf{B}\cdot(\mathbf{E}\times\mathbf{v})}{|\mathbf{B}| c} + \frac{\gamma(\mathbf{E}\times\mathbf{v})^2}{2|\mathbf{B}|c^2} + \frac{\gamma \mathbf{B}\cdot\mathbf{B}_E}{|\mathbf{B}|} \right] dt + \frac{g_F}{|g_F|} \left[\frac{\mathbf{B}\cdot[\Delta\mathbf{B}\times(\mathbf{E}\times\mathbf{v})]}{c|\mathbf{B}|^3} \right]. \tag{2}$$

The first term, negligible for Na, arises from an EDM. The next two terms describe the $\mathbf{E}\times\mathbf{v}$ effect; the linear $\mathbf{E}\times\mathbf{v}$ term is largely canceled by using the counterpropagating beams. This term is strictly velocity independent, since $\mathbf{v}dt = d\mathbf{r}$. The systematic error due to the quadratic $\mathbf{E}\times\mathbf{v}$ term is negligible, since it requires imperfect reversal of both $\mathbf{E}$ and $\mathbf{B}$. The fourth term describes the effect of a magnetic field $\mathbf{B}_E$ correlated with $\mathbf{E}$, such as might be generated by leakage and/or charging currents, effects of the HV reversal on the magnetic shields or power supplies, etc. The last term, odd in g_F, accounts for a geometric phase effect [15] that arises when the $(\mathbf{E}\times\mathbf{v})$-induced motion of the quantizing axis couples to an unintended magnetic field change $\Delta\mathbf{B}$ between the entrance and exit of the E field.

The coefficients A_k of Eq. (1) describe how well $\mathbf{B}_{\rm rf}$ achieves the $\pi/2$-pulse condition. In addition, A_1 ($F = 1$) and $A_1 - A_3$ ($F = 2$) depend upon quadratic corrections to the Zeeman splittings due to hyperfine mixing ($\propto \mathbf{B}^2$) and tensor Stark shifts ($\propto \mathbf{E}^2$) [11,12]. Thallium's large tensor Stark shift, 800 Hz at our E field, makes this dependence a useful diagnostic tool.

In thallium the measurement proceeds as follows. After the optical and rf resonances have been located, the machine is cycled through 128 different configurations: eight rf phases α [$\pm(90° \pm 45° \pm 1°)$], two $\mathbf{E}$ polarities, two atomic beam directions, two high-voltage (HV) cable polarities, and two $\mathbf{B}$ polarities; see Fig. 2. (The associated full periods are 75–150 ms for the rf, 3 s for $\mathbf{E}$, ~1 min for the beams, ~1.5 h for the cables, and ~3 h for $\mathbf{B}$.) Since there are also east and west atomic beams, 256 independent linear combinations can be constructed. An EDM would

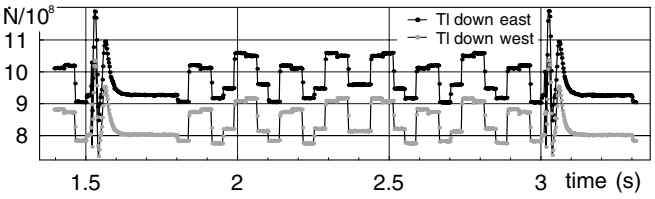

FIG. 2. This plot of typical raw data ($\dot{N}/10^8$ vs t/s) shows two $\mathbf{E}$ switches and the intervening 32 rf phase chops. (The 8 rf phases are cycled twice, and then twice again in reversed order.) The decaying quadratic Stark shift oscillations give proof of a switching $\mathbf{E}$ field of the claimed magnitude.

appear in the linear combination of signals that is odd (i.e., antisymmetric), even (i.e., symmetric), even, odd, even, odd, odd, and odd under the reversals just described and east/west exchange, respectively. [This symmetry can be worked out from Eqs. (1) and (2): the rf chops isolate the "magnetic" phase, and the EDM portion is $\propto \mathbf{E}\cdot\mathbf{B}$.] Other combinations provide useful diagnostic information. For instance, a $\pm 45°$-odd combination shows the quadratic Stark effect, and a $\pm 1°$-odd combination provides a normalization for each beam which is used to convert the raw linear combinations into calibrated phases. The EDM-like phase is $\delta \equiv (\varepsilon_{\rm east} - \varepsilon_{\rm west})/2$. Its east/west symmetric counterpart is labeled Σ. For sodium the procedure is identical except that there are only 2 rf phase chops [$\pm(151° \pm 1°)$], since the quadratic Stark shifts are too small to be interesting; and g_F is reversed by employing either F state.

The EDM data consist of 44 sets obtained on six nights in the year 2000. (Despite careful shielding, environmental magnetic noise prevented daytime data taking.) Each set had 32–64 beam periods (bp), with ~45 bp/set on average. The average current per detector was $\dot{N} \simeq 8.5 \times 10^8 e/$s. In 1988 bp (~35 h) with a run-time duty cycle of 0.55, we collected $\simeq 5.2 \times 10^{13} e$ per up/down beam pair. Table I summarizes the raw results, with uncertainties calculated assuming Gaussian statistics. In δ they are only 1.7 times the shot-noise limit. In Σ, which is vulnerable to magnetic interference from the local electric train system BART [16] and other sources, the uncertainty is substantially larger.

Despite excellent up/down beam cancellation, the motional field residuals are not negligible and require a correction. The EDM-like $\mathbf{E}\times\mathbf{v}$ systematic has the form

$$\varepsilon_{\mathbf{E}\times\mathbf{v}} \simeq \frac{g_F \mu_B}{2\hbar c} \int_{-L/2}^{L/2} (\Delta\mathbf{r}_{\rm ud}\cdot\nabla) \frac{\mathbf{B}\cdot(\mathbf{E}\times\mathbf{v})}{|\mathbf{B}| v_x}\, dx\,. \tag{3}$$

Since the atoms move in the x direction, the distance between the up and down beams $\Delta\mathbf{r}_{\rm ud}$ has only y and z components. With x-even and x-odd versions the total number of displacement types is four, each of which couples to a different set of field gradients.

To control the $\mathbf{E}\times\mathbf{v}$ residuals we take EDM-type data with the atomic beams cut such that each of the four displacements is individually enhanced. We then apply gradients in B_z and measure rf resonance frequency differences

TABLE I. Raw EDM-like phases, in units of 10^{-7}. These are the linear combinations with respect to reversals of the magnetic field (**B**) and high voltage cables (**C**) of the uncorrected, **E**-odd, up/down-even thallium phases ε. The **B**-even, **C**-odd effects are geometric phase residuals stemming from the $\Delta\mathbf{B}$ produced by the coils (i.e., the $\Delta\mathbf{B}$ that reverses with **B**), and do not contribute substantial correction to the final result.

B	**C**	$\varepsilon_{\text{east}}$	$\varepsilon_{\text{west}}$	δ	Σ
even	even	-3.1 ± 2.5	0.7 ± 2.4	-1.3 ± 1.4	-1.3 ± 2.0
odd	even	2.2 ± 2.5	3.2 ± 2.4	-0.8 ± 1.4	3.0 ± 2.0
even	odd	1.8 ± 2.5	-10.6 ± 2.4	6.2 ± 1.4	-4.2 ± 2.0
odd	odd	8.8 ± 2.5	8.4 ± 2.4	-0.4 ± 1.4	8.6 ± 2.0

$\delta\nu = \nu_{\text{up}} - \nu_{\text{down}}$ to determine these displacements. Similar measurements done during EDM data relate the spurious displacements to the enhanced ones. Then Eq. (3) reduces to

$$\varepsilon_{\mathbf{E}\times\mathbf{v}} = \sum_{\text{displacements}} \varepsilon_{\text{cut}} \frac{\delta\nu_{\text{uncut}}}{\delta\nu_{\text{cut}}}, \tag{4}$$

which involves only measured quantities.

Table II summarizes [17] the measurements of ε with the atomic beams cut in half. The $\varepsilon_{\delta y}$ and $\varepsilon_{\delta z}$ were reduced by gradient trimming prior to these measurements. Since the beams are not on the $z = 0$ symmetry axis, an east/west-odd $\partial B_z/\partial z$ was present before the turn number ratio between two pairs of B_z coils at different $|z|$ positions was adjusted. Wedging of the center electrode relative to the outer ones by a small angle $\sim 2 \times 10^{-4}$ created a $\partial E_y/\partial z$. The quadrupoles electronically corrected this tiny mechanical imperfection, reducing the mean $\partial E_y/\partial z$ by 80%. They could also have corrected an x-odd $\partial E_y/\partial z$, had it been necessary.

Since the atomic beam slits could have clogged at any time, the relatively rapid measurements of $\delta\nu_{\text{uncut}}$ were done twice each night. In all cases the average uncut displacements were less than 3% of the cut ones, implying that the ε's from Table II are suppressed by a factor of 30 or more in the real EDM data. For both beams the largest contribution to $\varepsilon_{\mathbf{E}\times\mathbf{v}}$ comes from the product of the x-odd δy and the x-odd $\partial B_y/\partial y$, which unfortunately was untrimmed. The mean $\mathbf{E} \times \mathbf{v}$ contributions to the measured phase total -0.2 ± 1.1 and -2.0 ± 1.2, in units of 10^{-7}, for the east and west beams, respectively.

With large fluxes Tl and Na compete to leave the ovens. We generally favored thallium to sodium's detriment, limiting the utility of Na as a comagnetometer. However, because the geometric phase effect ε_{geo} scales linearly with velocity, Na is three times more sensitive to ε_{geo}, and it has the g_F handle. Thus we first studied ε_{geo} (by taking data at low **B**) with Na. The data did not present a consistent picture. Experimental, analytic, and numerical follow-up investigations elucidated a new type of systematic. Proportional to the product of a laser polarization misalignment and the nonadiabatic portion of the transition into or out of the E field, this effect is **B**-even and substantial only in Na at low field.

We thus also used thallium to study ε_{geo}. Table III shows data from both Na and Tl, scaled in accordance with the **B**-odd geometric phase hypothesis (assumes $\Delta\mathbf{B}$ due to a source other than the coils). The **B**-odd scaling $\sim v/B^2$ [see Eq. (2)] is fairly well supported in Σ, but the discrepancies in δ are significant. The values finally adopted for ε_{geo} are the combination of the three sets of low field data shown. Because the agreement is unsatisfactory, we have enlarged the uncertainty sufficiently to make the three values consistent. Even though the east/west-odd ΔB_x is uncorrected, Σ here is comparable to or smaller than δ, implying that the source of the nonreversing $\partial B_x/\partial x$ is distant from the atomic beams.

After correcting the raw data for the $\mathbf{E} \times \mathbf{v}$ and geometric phase effects, we have $\delta = -1.8 \pm 1.6$ and $\Sigma = 9.5 \pm 3.6$ (in units of 10^{-7}). The uncertainty in δ is straightforward since the data are normally distributed. The final uncertainty in Σ, susceptible to common-mode interference, is determined from a χ^2 analysis and reflects the presence of outlying values and night-to-night fluctuations in the raw data not expected for a normal distribution. See Tables IV and V. While there is no evidence of an EDM, the significant Σ indicates an as-yet unexplained effect whose possible effect on δ must be considered.

TABLE II. $\mathbf{E} \times \mathbf{v}$ gradient summary. ε_{cut} is given in units of 10^{-7} and $\delta\nu_{\text{cut}}$ in Hertz. The $\delta\nu$ are all assigned an uncertainty (systematic) of 0.1 Hz. Subscripts even/odd refer to x-reflection symmetry about the midplane of the apparatus.

Disp.	Dominant gradient	Tl east ε_{cut}	Tl east $\delta\nu_{\text{cut}}$	Tl west ε_{cut}	Tl west $\delta\nu_{\text{cut}}$
$\delta z\|_{\text{even}}$	$dE_y/dz\|_{\text{even}}$	37 ± 19	7.9	27 ± 17	8.2
$\delta z\|_{\text{odd}}$	$dE_y/dz\|_{\text{odd}}$	-45 ± 11	8.7	14 ± 13	8.5
$\delta y\|_{\text{even}}$	$dBy/dy\|_{\text{even}}$	-15 ± 15	10.1	24 ± 16	10.2
$\delta y\|_{\text{odd}}$	$dBy/dy\|_{\text{odd}}$	84 ± 15	17.1	-113 ± 19	16.6

TABLE III. Low-field, **B**-odd, cable-odd effects scaled assuming $\varepsilon = \varepsilon_{\text{geo}}$ to their expected values in Tl at 179 kHz, in units of 10^{-7}. The sodium data reflect only the g_F-odd effect. These data were taken after a corrective gradient of $\partial B_x/\partial x \sim 10^{-6}$ G/cm was applied. Γ is the suppression factor that extrapolates the measured phase to Tl at 179 kHz.

Low field	$\|\mathbf{B}\|$ [mG]	ν [kHz]	Γ	δ	Σ
10 July Na	90	63.3	53.8	0.5 ± 0.3	-0.4 ± 0.5
15 Aug Tl	90	42.0	18.1	1.1 ± 0.2	0.7 ± 0.4
23 Aug Tl	60	27.9	41.0	-0.1 ± 0.2	0.3 ± 0.5
Adopted Tl	380	178.6	1.0	0.5 ± 0.5	0.3 ± 0.5

TABLE IV. Σ data and corrections for each night.

		$\Sigma[10^{-7}]$			
Date	$\lvert\mathbf{B}\rvert$[mG]	Raw	$\mathbf{E}\times\mathbf{v}$	Geometric	Total
12-Jul	380	16.8 ± 5.0	1.4 ± 0.8	-0.27 ± 0.5	17.9 ± 5.1
13-Jul	380	2.7 ± 5.1	2.0 ± 0.9	-0.27 ± 0.5	4.4 ± 5.2
15-Jul	380	1.9 ± 4.3	0.8 ± 0.7	-0.27 ± 0.5	2.4 ± 4.4
12-Aug	380	1.6 ± 4.8	0.8 ± 0.7	-0.27 ± 0.5	1.9 ± 4.9
30-Aug	380	10.3 ± 5.9	1.5 ± 0.8	-0.27 ± 0.5	11.5 ± 6.0
24-Sep	760	19.7 ± 4.6	0.4 ± 0.8	-0.07 ± 0.13	20.0 ± 4.7
Mean		8.6 ± 3.5	1.1 ± 0.8	-0.24 ± 0.44	9.5 ± 3.6

The cause of Σ is almost certainly a $\mathbf{B}_E \sim 10^{-10}$ G $\hat{\mathbf{z}}$. The most plausible $\mathbf{B}_E$ scenarios involve distant sources (magnetic shields, power supplies) and therefore give negligible $|\delta/\Sigma|$. Pathological currents in the quadrupole assemblies have been ruled out. However, 10 nA in the main electrodes could produce the required east/west-even B_E with a non-negligible east/west-odd component.

To place a limit on leakage currents we charge the E-field plates to high voltage and then disconnect them from the supplies. Decay of the electrode voltage is observed via the quadratic Stark shift asymmetry. Repeated measurements show a current $\lesssim$2 nA, with the probable leakage path remote from the atomic beams.

Charging currents are also determined by means of the Tl quadratic Stark effect, which is isolated by the rf chops alone. Thus there are four independent measurements of the E field per $\mathbf{E}$ switch. Binning the quadratic Stark asymmetry by time-after-$\mathbf{E}$ chop shows a decaying charging current with an average value of 2 nA. Binning the ε's similarly reveals no evidence of time dependence [18].

Dielectric absorption (DA) in the insulators that support the electrodes could lead to a current with a time constant $\gtrsim$1 s and $\lesssim$1 h, which would evade the tests described already. Traditional electronic methods render this model implausible, but do not exclude it completely. Numerical calculations give $|\delta/\Sigma| < 0.16$ for all possible single current paths, with an average value of 0.11. Taking into consideration the possible sources of B_E, we believe $|\delta/\Sigma| \leq 0.11$ is a very conservative upper bound.

TABLE V. δ data and corrections for each night.

		$\delta[10^{-7}]$		
Date	Raw	$\mathbf{E}\times\mathbf{v}$	Geometric	Total
12-Jul	-5.2 ± 3.3	-1.2 ± 0.8	-0.5 ± 0.5	-6.9 ± 3.4
13-Jul	-3.8 ± 4.3	-0.6 ± 0.9	-0.5 ± 0.5	-4.8 ± 4.4
15-Jul	2.8 ± 3.0	-1.4 ± 0.7	-0.5 ± 0.5	0.9 ± 3.1
12-Aug	-1.6 ± 3.4	-0.6 ± 0.7	-0.5 ± 0.5	-2.6 ± 3.5
30-Aug	-0.3 ± 3.4	-0.2 ± 0.8	-0.5 ± 0.5	-1.0 ± 3.5
24-Sep	3.5 ± 3.3	-1.5 ± 0.8	-0.12 ± 0.13	1.8 ± 3.4
Mean	-0.4 ± 1.4	-0.9 ± 0.8	-0.43 ± 0.46	-1.8 ± 1.6
	With Σ contribution to error			-1.8 ± 1.9

Model-independent δ/Σ correlation analyses show no correlation and negligible impact of Σ on the δ uncertainty. The non-Gaussian variability of Σ actually increases the power of this method. Despite these arguments, we include a Σ contribution to the δ uncertainty since the DA model has not been excluded. See Table V.

Using $\bar{v} = 4.2 \times 10^4$ cm/s (measured two different ways), $R = -585$, and $E = 410$ statvolts/cm, we find that the final value for δ given in Table V implies $d_e = (6.9 \pm 7.4) \times 10^{-28} e$ cm. The limit is $|d_e| \leq 1.6 \times 10^{-27} e$ cm with 90% confidence.

We thank machinist A. Vaynberg and electronics engineer J. Davis for excellent work, and A. T. Nguyen, D. Budker, J. Clarke, Y. Zhang, and R. Falcone for useful discussions and assistance. We also gratefully acknowledge excellent work by the late machinists A. Brocato and S. Bonilla, and numerous technical contributions by the late Lars Commins. This work was supported by the Director, Office of Science, of the U.S. Department of Energy under Contract No. DE-AC03-76SF00098.

*Electronic address: regan@physics.berkeley.edu
†Electronic address: commins@physics.berkeley.edu
‡Electronic address: christian.j.schmidt@de.abb.com
§Electronic address: david.demille@yale.edu

[1] L. Landau, Sov. Phys. JETP **5**, 336 (1957).
[2] A. Abashian *et al.,* Phys. Rev. Lett. **86**, 2509 (2001).
[3] M. E. Pospelov and I. B. Khriplovich, Sov. J. Nucl. Phys. **53**, 638 (1991).
[4] I. B. Khriplovich and S. K. Lamoreaux, *CP Violation Without Strangeness* (Springer, New York, 1997).
[5] E. D. Commins, in *Advances in Atomic, Molecular, and Optical Physics* (Academic Press, New York, 1999), Vol. 40, pp. 1–55.
[6] M. V. Romalis, W. C. Griffith, J. P. Jacobs, and E. N. Fortson, Phys. Rev. Lett. **86**, 2505 (2001).
[7] P. G. Harris *et al.,* Phys. Rev. Lett. **82**, 904 (1999).
[8] P. G. H. Sandars, Phys. Lett. **14**, 194 (1965).
[9] Z. W. Liu and H. P. Kelly, Phys. Rev. A **45**, R4210 (1992).
[10] K. Abdullah, C. Carlberg, E. D. Commins, H. Gould, and S. B. Ross, Phys. Rev. Lett. **65**, 2347 (1990).
[11] E. D. Commins, S. B. Ross, D. DeMille, and B. C. Regan, Phys. Rev. A **50**, 2960 (1994).
[12] B. C. Regan, Ph.D. thesis, Physics Department, University of California, Berkeley, 2001, available from the author or http://www.umi.com
[13] N. F. Ramsey, *Molecular Beams* (Oxford University Press, London, 1956), Chap. V, Sec. 4, and references therein.
[14] W. T. Welford and R. Winston, *High Collection Nonimaging Optics* (Academic Press, San Diego, 1989).
[15] E. D. Commins, Am. J. Phys. **59**, 1077 (1991).
[16] A. C. Fraser-Smith and D. B. Coates, Radio Sci. **13**, 661 (1978).
[17] "Summarize" in this case means the displacement-odd, **B**-odd, and cable-odd component; the other linear combinations are generally not significant.
[18] This point also argues against any effect caused by the shields, which are observed to have a 70 ms time constant.